University of Glasgow
DEPARTMENT OF
AEROSPACE
ENGINEERING

Identification of Gyroplane Lateral/Directional Stability and Control Characteristics From Flight Test

S. S. Houston

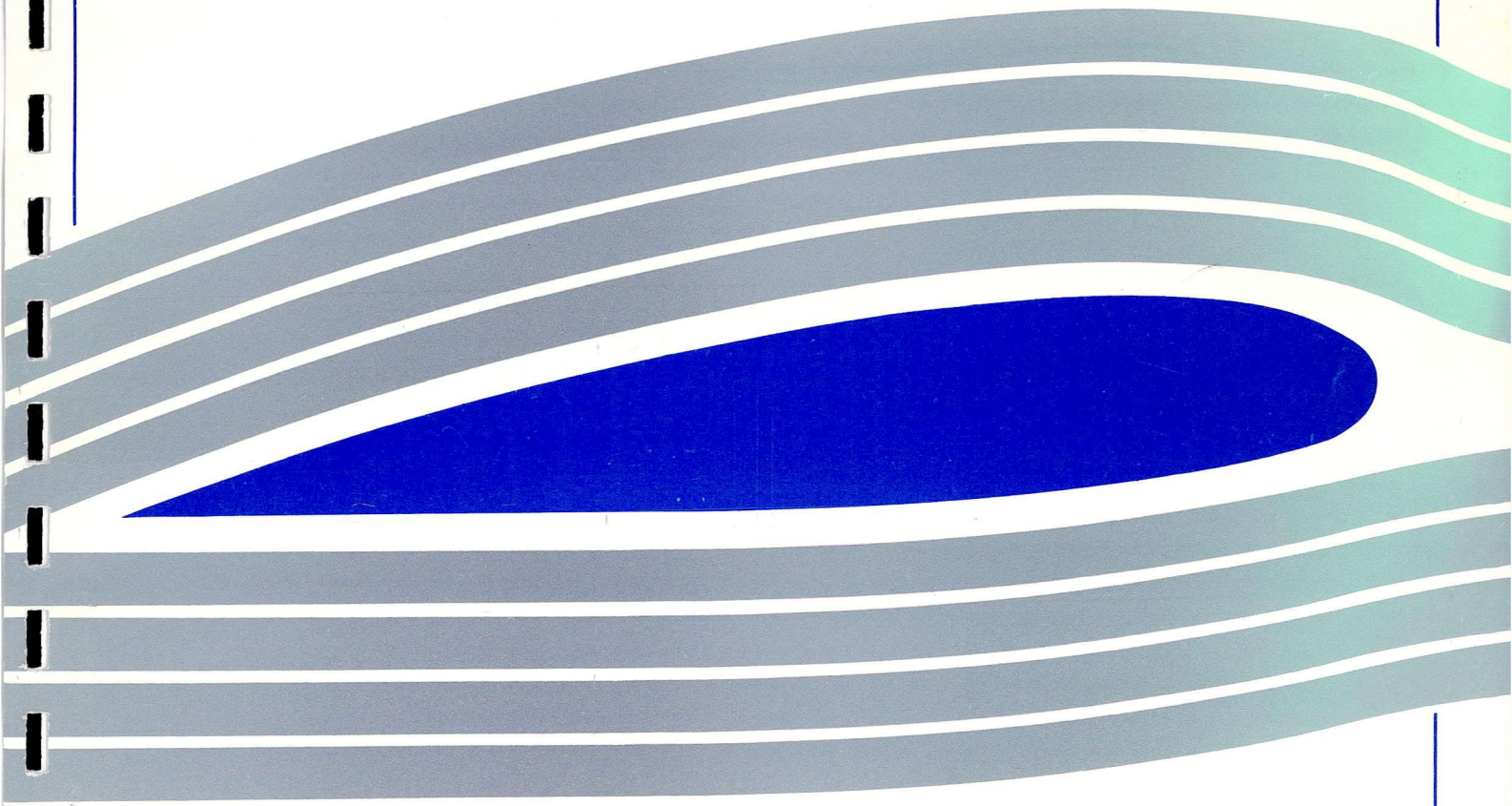

Identification of Gyroplane Lateral/Directional Stability and Control Characteristics From Flight Test

S. S. Houston

Dept. of Aerospace Engineering

Report No. 9710

Identification of Gyroplane Lateral/Directional Stability and Control Characteristics From Flight Test

S. S. Houston[1]

Abstract

This Paper presents an analysis of test data recorded during flight trials of a gyroplane. This class of rotary-wing aircraft has found limited application in areas other than sport or recreational flying. However, the accident rate is such that a study of the configuration's stability and control characteristics is timely, and in addition substantive data is required for a new airworthiness and design standard that is under development. The Paper complements previous work on the longitudinal degrees of freedom and as a consequence, serves to complete the definitive analysis of gyroplane stability and control. The identified derivatives are related to specific aspects of the layout of the gyroplane, and hence the influence of design on the static and dynamic behaviour is quantified. It is concluded that robust estimates of the lateral and directional stability and control derivatives have been identified, indicating benign and "conventional" characteristics.

[1]Member R.Ae.S.
Lecturer, Dept. of Aerospace Engineering
The University of Glasgow
Glasgow
Scotland
G12 8QQ

Nomenclature

A, B	state-space system and control matrices
i	imaginary operator
L_v, L_p, etc	rolling acceleration derivatives, 1/(ms), 1/s etc.
N_v, N_p, etc	yawing acceleration derivatives, 1/(ms), 1/s etc.
$p,\ r$	angular velocity components about x, z body axes, rad/s
R	correlation coefficient
Re[], Im[]	real and imaginary components of []
V_f	airspeed, m/s
v	velocity component along lateral body axis, m/s
v_{probe}	velocity component along lateral air data probe axis, m/s
$\underline{x}, \underline{u}$	state and control vectors
$\underline{x}(\omega), \underline{u}(\omega)$	Fourier-transformed state and control vectors
$x_{vane},\ z_{vane}$	sideslip vane location in body axes, m
$x_{cg},\ z_{cg}$	aircraft centre-of-mass position in body axes, m
Y_v, Y_p, etc	lateral body axis acceleration derivatives, 1/s, m/(rad s), etc.
β_{vane}	sideslip measured at vane location, rad
Δf	frequency increment, rad/s
Δt	time increment, s
η_c	lateral stick position, % (0% fully left)
η_{ped}	rudder pedal position, % (0% fully left)
ω	frequency, rad/s

Introduction

There are a wide range of configurations in the class of aircraft known as rotorcraft. The helicopter is the most common type, finding widespread application in commercial and military aviation. The gyroplane (or autogyro), however, is an increasingly popular machine in sport and recreational flying, having found no practical application in contemporary commercial or military roles.

Currently, most if not all types of gyroplane are in the homebuilt, or experimental category. The study of the configuration's flight mechanics is timely, given the accident rate suffered by the aircraft, e.g. Ref. 1. This, together with the increase in light gyroplane flying in the U.K., has heightened interest in this class of aircraft, and a new airworthiness and design standard (BCAR Section T) has been published by the U.K. Civil Aviation Authority, Ref. 2.

However, there is little substantive data at present to support the design standard, and the literature has not, until recently, addressed stability and control (Refs. 3, 4). The objective of this Paper is therefore to contribute to a sparse literature on the subject of gyroplane flight mechanics, thereby directly supporting BCAR Section T. The specific aims of the work are: to explore the application, to the gyroplane, of previous research in rotorcraft system identification; to obtain robust estimates of lateral/directional stability and control derivatives; and to use these derivatives to assess the nature of the flight dynamics of gyroplanes.

Background

The gyroplane helped to pave the way for the development of the helicopter, introducing cyclic pitch control and blades attached to the rotor hub by means of a hinge. However, it is only recently that stability and control issues have been addressed in the literature, Refs. 3 and 4. This recent work considered longitudinal stability and control. It has shown that gyroplanes can exhibit conventional stability and control characteristics, although the rotorspeed degree of freedom couples strongly with the classical short-period and phugoid modes of motion. Prior to that work, the literature on gyroplanes nonetheless is considerable, Refs. 5-15 for example. However, in a contemporary context, this work is now primarily of historical significance. It provides the basis of the understanding of gyroplane flight, but does not address the issues of stability and control. Examination of the literature shows a logical development of the study of gyroplanes, from the elementary theory of gyroplane flight, to an analysis of aerodynamics and performance and ultimately rotor behaviour, but only for steady flight. Interest then apparently waned and the next logical stage in the study of the gyroplane i.e. stability and control, was not examined. For example, the work of Glauert includes the derivation of simple expressions for rotorspeed as a function of loading and axial velocity, Ref. 5. Wheatley, Ref. 11 derived expressions for the flapping angles required for equilibrium flight, presenting results that show how coning, longitudinal and lateral flap angles vary with flight condition. Nowadays, these analyses would be recognisable as classical rotary-wing theory and analogous to that found in helicopter text books. Wheatley even examined higher harmonic components of blade flapping behaviour, Ref. 13.

It is in this context that gyroplane flight trials and the associated data analysis methods were planned. There is an extensive literature on system identification and parameter estimation, and application to the rotorcraft problem is well documented,

e.g. Refs. 16-21. Tischler in particular has argued strongly in favour of the merits of frequency-domain identification, specifically directed towards the synthesis of non-parametric frequency responses. The repeatability and consistency achieved indicates that the frequency domain approach is robust.

The approach taken in this Paper is to adopt a frequency-domain equation-error method using linear regression, to synthesise conventional 3 degree-of-freedom stability and control derivatives. This model structure is familiar to flight dynamicists, thereby facilitating general insight into fundamental behaviour of the gyroplane. Specific derivatives are directly related to individual, or group, effects that would otherwise be hidden in the aggregate presentation of a frequency response. The equation error method has limitations, as described in Refs. 16 and 19, although working in the frequency domain minimises some of the difficulties. The advantage is the simplicity of the approach, in concept and application. It is argued that good results can be obtained with a frequency-domain equation-error approach if careful design of the experiments, the equipment installation and execution of the flight trials is complemented by sound engineering judgement applied to the interpretation of the data.

Aircraft and Experimental Installation

The aircraft used in this study was the VPM M16 gyroplane, Figure 1. It is of Italian origin, produced in kit form for assembly by the owner. The maximum all-up mass is 450 kg. The aircraft is powered by a four-cylinder two-stroke engine driving a three-bladed fixed pitch propeller. For helicopter engineers not familiar with gyroplanes, the rotor system is of an interesting configuration, typical of this class of aircraft. The two main rotor blades are bolted to a teeter bar, suspended from a teeter bolt. The blades are untwisted, and no cyclic pitch can be applied. This hub assembly is mounted on a spindle, about 200mm long, and this spindle pivots about its lower end to tilt the entire rotor fore and aft and laterally to effect pitch and roll control, respectively. In this regard, the aircraft could be classed as a tilt-rotor.

The experimental installation consisted of a digital on-board recording system, operating at 10 Hz. A nose-mounted air data probe containing sideslip and angle of attack vanes was fitted, and an inertial unit measured angular velocities about three axes, and linear accelerations along these axes. A separate unit was used to measure roll and pitch angles . Pilot control positions were measured using potentiometers. Rotorspeed was also recorded. The front seat and flight controls were removed to accommodate the system.

The gyroplane presents a particular challenge, in addition to those normally met with helicopter system identification. The aircraft is light, which demands stringent limits on atmospheric conditions during the tests. Solo operation of this aircraft was essential due to the mass and space restrictions imposed by the instrumentation system. This placed particular demands on the test pilot's flying skills in order that the quality of test input was not compromised.

Data Analysis and Model Synthesis

The model structure for which coefficients are to be identified, is of conventional state-space form, i.e.

$$\dot{\underline{x}} = A\underline{x} + B\underline{u}$$

where

$$A = \begin{bmatrix} Y_v & Y_p & Y_\phi & Y_r & 0 \\ L_v & L_p & 0 & L_r & 0 \\ 0 & 1 & 0 & 0 & 0 \\ N_v & N_p & 0 & N_r & 0 \\ 0 & 0 & 0 & 1 & 0 \end{bmatrix} \quad , \quad B = \begin{bmatrix} Y_{\eta_c} & Y_{\eta_{ped}} \\ L_{\eta_c} & L_{\eta_{ped}} \\ 0 & 0 \\ N_{\eta_c} & N_{\eta_{ped}} \\ 0 & 0 \end{bmatrix}$$

This constitutes the lateral/directional subset of the conventional 6 degree-of-freedom rigid-body flight mechanics model. The rigid body states are taken to be with respect to the usual mutually orthogonal, right-handed frame of reference whose origin is at the centre of mass.

The angular quantities in the state vector, and the control positions, are all measured directly. The translational velocity v is obtained from airspeed and sideslip data measured at the nose-mounted boom, as follows.

$$v = v_{probe} - p(z_{vane} - z_{cg}) + r(x_{vane} - x_{cg})$$

and

$$v_{probe} = V_f \sin\beta_{vane}$$

The time histories of each variable were then converted into frequency domain information using a Discrete Fourier Transform, Ref. 21, given by

$$X(k\Delta f) = \Delta t \sum_{n=0}^{N-1} x_n e^{-i2\pi(kn)/N}; \quad k = 0,1,2,\ldots,N-1$$

which gives real and imaginary parts of X ,

$$\mathrm{Re}[X(k\Delta f)] = \Delta t \sum_{n=0}^{N-1} x_n \cos(2\pi(kn)/N); \quad \mathrm{Im}[X(k\Delta f)] = -\Delta t \sum_{n=0}^{N-1} x_n \sin(2\pi(kn)/N)$$

The quality of these frequency domain data can be enhanced by standard processing techniques such as applying overlapped and tapered windows to the data, as recommended by Tischler, Ref. 21.

Each degree of freedom can then be treated separately, and formulation as a linear regression problem allows estimation of the coefficients. The state-space description is converted to the frequency domain, i.e.

$$i\omega\, \underline{x}(\omega) = A\underline{x}(\omega) + B\underline{u}(\omega)$$

Note that this assumes that any process noise is zero. The real parts on each side can be equated, as can the imaginary parts, to give two matrix equations that the A and B coefficients must satisfy, viz.

$$-\omega\,\mathrm{Im}[\underline{x}(\omega)] = A(\mathrm{Re}[\underline{x}(\omega)]) + B(\mathrm{Re}[\underline{u}(\omega)])$$
$$\omega\,\mathrm{Re}[\underline{x}(\omega)] = A(\mathrm{Im}[\underline{x}(\omega)]) + B(\mathrm{Im}[\underline{u}(\omega)])$$

The rolling moment equation for example, is then expressed as the two equations

$$-\omega \,\mathrm{Im}[p(\omega)] = L_v \,\mathrm{Re}[v(\omega)] + L_p \,\mathrm{Re}[p(\omega)] + L_r \,\mathrm{Re}[r(\omega)] + L_{\eta_c} \,\mathrm{Re}[\eta_c(\omega)] + L_{\eta_{ped}} \,\mathrm{Re}[\eta_{ped}(\omega)]$$

$$\omega \,\mathrm{Re}[p(\omega)] = L_v \,\mathrm{Im}[v(\omega)] + L_p \,\mathrm{Im}[p(\omega)] + L_r \,\mathrm{Im}[r(\omega)] + L_{\eta_c} \,\mathrm{Im}[\eta_c(\omega)] + L_{\eta_{ped}} \,\mathrm{Im}[\eta_{ped}(\omega)]$$

The other degrees of freedom are in a similar form.

The equation-error formulation is especially useful in circumstances where not all the degrees of freedom in the model structure can be identified from a single event. In such cases the rolling moment, for example, identified from one flight or event can be incorporated in the state-space model structure with the sideforce or yawing moment equations identified from another.

Results

Frequency sweep inputs were performed on rudder and lateral stick controls at a nominal airspeed of 70 mph. These data were used for identifying the stability and control derivatives. Doublet inputs were also applied to these controls to provide dissimilar data for checking the veracity of the identified models. Figure 2 illustrates a typical frequency sweep performed with lateral stick, while Figure 3 shows a rudder pedal input. It is instructive to consider these data qualitatively before any processing is carried out. Note that the lateral stick input produces small yaw rates in relation to the roll rate generated, while the rudder input produces sideslip and yaw rate response, but an insignificant level of response in the roll degree of freedom.

An important aspect in any system identification study is the *identifiability* of the estimated parameters, Refs. 22, 23. This is particularly germane to the equation error approach. *Robust* estimates of the derivatives are those whose values can be judged to be invariant with the event, input type, estimation method or frequency range used, and for which a low standard error is calculated. *Verification* of the appropriateness of the identified model is usually achieved by confirming that it will predict the response to a dissimilar control input to that used in the identification. The issue of identifiability is of particular concern to the gyroplane problem as there is no literature on the vehicle's lateral/directional characteristics. These issues are explored next.

Derivative estimates from dissimilar controls types

Estimates of the sideforce derivatives obtained from lateral stick inputs, are compared with those obtained from rudder in Table 1. The standard error associated with each derivative is given in parentheses. These estimates were obtained by matching the model structure with the flight data over a 1 Hz frequency range.

Table 1 Y-force derivative comparison - dissimilar input types

parameter	lateral stick input	rudder pedal input
R^2	0.691	0.924
Y_v	0.148 (0.069)	-0.046 (0.025)
Y_p	-1.661 (0.642)	-0.809 (1.812)
Y_ϕ	11.111 (0.514)	28.8345 (5.115)
Y_r	-34.176 (1.802)	-34.755 (0.971)
Y_{η_c}	-0.009 (0.012)	-0.009 (0.027)
$Y_{\eta_{ped}}$	0.187 (0.035)	0.065 (0.017)

The correlation coefficient indicates that the data from the rudder input is the most appropriate to use with this model structure. The standard error associated with Y_p and Y_ϕ is large, indicating low confidence in the value of the derivative. These terms can be left out of the model structure as insignificant. This is of some concern with regard to Y_ϕ, as it is one of two derivatives in this degree of freedom that physically ought to have negligible aerodynamic or propulsion force contributions (i.e. those dominated by kinematic or gravitational terms), the other being Y_r. The former ought to have a value of approximately 9.81. It can be seen that in this respect, the lateral stick frequency sweep paradoxically offers a much better estimate of Y_ϕ than the data generated with the rudder pedal sweep. These identifiability issues are consistent with Figure 3 where it is clear that rudder inputs produce very little roll disturbance, i.e. there is insufficient data to accurately identify derivatives with respect to roll. However, both input types give estimates of Y_r that are consistent with the mean flight speed of 34 m/s.

The evidence would therefore suggest that the most appropriate course of action is to use the rudder pedal frequency sweep data, but with a revised model structure that does not contain Y_p, Y_ϕ or Y_{η_c}. Table 2 shows the result.

Table 2 Y-force derivative estimates from rudder pedal frequency sweep - revised model structure

parameter	estimate
R^2	0.915
Y_v	-0.081 (0.022)
Y_r	-32.538 (0.761)
$Y_{\eta_{ped}}$	0.043 (0.015)

In the state-space model, the derivative Y_ϕ is set to the physically-correct value of 9.80665, with Y_p and Y_{η_c} set to zero as the results suggest that they cannot be estimated with any confidence.

Corresponding estimates of the rolling moment derivatives obtained from lateral stick inputs, are compared with those obtained from rudder in Table 3. The standard error associated with each derivative is given in parentheses.

Table 3 rolling moment derivative comparison - dissimilar input types

parameter	lateral stick input	rudder pedal input
R^2	0.882	0.060
L_v	0.047 (0.010)	-0.001 (0.003)
L_p	-2.407 (0.090)	-0.144 (0.206)
L_r	0.169 (0.252)	-0.112 (0.111)
L_{η_c}	0.069 (0.002)	-0.001 (0.002)
$L_{\eta_{ped}}$	-0.003 (0.005)	0.005 (0.003)

Unlike the sideforce derivatives, in this instance the rudder pedal sweep data is clearly inappropriate, in several respects. The correlation coefficient is too small, indicating a poor model structure; the standard error for each parameter is very large

in relation to the parameter estimates; and inspection of Figure 3 again shows qualitatively that rudder inputs produce insignificant amounts of roll response. By contrast, the lateral stick frequency sweep data gives derivatives with a very low standard error, with the exception of L_r and $L_{\eta_{ped}}$. In the latter case this is due to the fact that there is an insignificant level of rudder activity during the lateral sweep, while in the former it is because there is little yaw rate response to lateral stick displacement, as seen from Figure 2.

These results suggest that the roll moment model structure should be modified to neglect L_r and $L_{\eta_{ped}}$. Table 4 shows the result.

Table 4 rolling moment derivative estimates from lateral stick frequency sweep - revised model structure

parameter	estimate
R^2	0.882
L_v	0.050 (0.004)
L_p	-2.438 (0.082)
L_{η_c}	0.069 (0.002)

The very small standard error relative to the corresponding derivative estimate is a measure of the high degree of confidence in the estimated values.

Finally, estimates of the yawing moment derivatives obtained from lateral stick inputs, are compared with those obtained from rudder in Table 5. In this case, the results from the lateral stick frequency sweep can be discarded, once again on the basis of the correlation coefficient alone. This is consistent with Figure 2 which shows limited yawing response to lateral stick inputs. The rudder frequency sweep result indicates that N_p can be discarded from the model structure due to the relatively high standard error associated with the estimate. Again, this is consistent

with Figure 3 where there is negligible roll rate response to rudder inputs. The revised parameter estimates are given in Table 6.

Table 5 yawing moment derivative comparison - dissimilar input types

parameter	lateral stick input	rudder pedal input
R^2	0.588	0.912
N_v	0.039 (0.003)	0.059 (0.002)
N_p	-0.214 (0.030)	0.066 (0.168)
N_r	-0.426 (0.088)	-0.939 (050)
N_{η_c}	0.020 (0.001)	-0.002 (0.004)
$N_{\eta_{ped}}$	0.006 (0.001)	0.032 (0.001)

Table 6 yawing moment derivative estimates from rudder pedal frequency sweep - revised model structure

parameter	estimate
R^2	0.882
N_v	0.060 (0.001)
N_r	-0.931 (0.044)
$N_{\eta_{ped}}$	0.032 (0.001)

Derivative estimates from fits over dissimilar frequency ranges

Suitable choice of frequency range across which the identification is to be conducted, is important for two reasons. First, too small a frequency range and insufficient information may be available to fully specify the parameters in the model structure. Second, too large a frequency range, and dynamics unmodelled by the 3 degree-of-freedom structure may distort the values. Derivative estimates from the frequency sweep data were obtained by regression over 0.5 Hz and these results

are compared in Tables 7-9 with those obtained previously for a frequency range of 1 Hz.

Table 7 Y-force derivative estimates from rudder pedal frequency sweep - revised model structure, dissimilar frequency range

parameter	estimate, 0.5 Hz	estimate, 1.0 Hz
R^2	0.953	0.915
Y_v	-0.089 (0.023)	-0.081 (0.022)
Y_r	-32.212 (0.792)	-32.538 (0.761)
$Y_{\eta_{ped}}$	0.035 (0.016)	0.043 (0.015)

Table 8 rolling moment derivative estimates from lateral stick frequency sweep - revised model structure, dissimilar frequency range

parameter	estimate, 0.5 Hz	estimate, 1.0 Hz
R^2	0.917	0.882
L_v	0.034 (0.003)	0.050 (0.004)
L_p	-2.582 (0.084)	-2.438 (0.082)
L_{η_c}	0.063 (0.002)	0.069 (0.002)

Table 9 yawing moment derivative estimates from rudder pedal frequency sweep - revised model structure, dissimilar frequency range

parameter	estimate, 0.5 Hz	estimate, 1.0 Hz
R^2	0.944	0.882
N_v	0.059 (0.002)	0.060 (0.001)
N_r	-0.904 (0.046)	-0.931 (0.044)
$N_{\eta_{ped}}$	0.031 (0.001)	0.032 (0.001)

Only the estimate for L_v shows the greatest relative difference between the 0.5 and 1 Hz regressions. The limited variability of the estimates with frequency range tend to suggest that the model structure is appropriate for frequencies up to 1 Hz.

Verification

The state-space model constructed from the identified derivatives in Tables 2, 4 and 6 is given by

$$\begin{bmatrix} \dot{v} \\ \dot{p} \\ \dot{\phi} \\ \dot{r} \\ \dot{\psi} \end{bmatrix} = \begin{bmatrix} -0.081 & 0 & 9.80665 & -32.538 & 0 \\ 0.050 & -2.438 & 0 & 0 & 0 \\ 0 & 1 & 0 & 0 & 0 \\ 0.060 & 0 & 0 & -0.931 & 0 \\ 0 & 0 & 0 & 1 & 0 \end{bmatrix} \begin{bmatrix} v \\ p \\ \phi \\ r \\ \psi \end{bmatrix} + \begin{bmatrix} 0 & 0.043 \\ 0.069 & 0 \\ 0 & 0 \\ 0 & 0.032 \\ 0 & 0 \end{bmatrix} \begin{bmatrix} \eta_c \\ \eta_{ped} \end{bmatrix}$$

The eigenvalues or stability roots of the system are given in Table 10, and are recognisable as roll subsidence, dutch roll and spiral modes of motion.

Table 10 identified lateral/directional model stability roots

mode	eigenvalue
roll	-2.382
dutch roll	-0.580±1.3133i
spiral	0.0923

Figure 5 shows verification of the model identified from frequency sweep data. The model is driven by a doublet-type input made with lateral stick displacements at the same nominal flight condition. The identified model provides a very good representation of the overall response. The influence of the unstable spiral mode is not clear, however.

Figure 6 shows verification of the model for rudder inputs. The identified model provides a very good representation of the short- to medium-term response, i.e. that dominated by roll subsidence and dutch roll. The influence of the unstable spiral mode is clear in this case however, with the longer term response of the model clearly diverging from the flight measurements, although not to a significant extent.

Analysis of spiral mode characteristics

The unstable spiral mode is inconsistent with the observed behaviour in any response data from rudder or lateral stick inputs, which shows no divergent tendency. Padfield, Ref. 24, presents an approximation to the spiral mode which shows that it is influenced by all of the lateral and directional stability derivatives. For $L_r = 0$ and $N_p = 0$, it reduces to

$$\lambda_{spiral} = \frac{g(L_v N_r)}{V_f (L_p N_v + g L_v / V_f)}$$

This approximation can be used to examine the nature of spiral mode, as it gives $\lambda_{spiral} = 0.113$, i.e. very close to the exact value in Table 10. Inspection of the approximation above shows that the stability of this mode is determined by the dihedral effect, L_v. Positive dihedral effect, $L_v < 0$ will tend to stabilise the spiral mode. Here, $L_v > 0$. Simple numerical sensitivity analysis using the identified state-space model confirms that reducing the magnitude of L_v reduces the magnitude of λ_{spiral}.

A statistical interpretation of the standard error is that it represents upper and lower bounds which define limits on the confidence and probability with which each derivative has been estimated. A factor of 1.97 applied to each standard error gives an upper and lower limit defining the boundaries for which there is 95% confidence that there is a 95% probability that the derivatives lies within that range. If the value

of each derivative is set at the appropriate bound for reducing λ_{spiral}, the state-space model becomes

$$\begin{bmatrix} \dot{v} \\ \dot{p} \\ \dot{\phi} \\ \dot{r} \\ \dot{\psi} \end{bmatrix} = \begin{bmatrix} -0.081 & 0 & 9.80665 & -34.035 & 0 \\ 0.041 & -2.599 & 0 & 0 & 0 \\ 0 & 1 & 0 & 0 & 0 \\ 0.063 & 0 & 0 & -0.845 & 0 \\ 0 & 0 & 0 & 1 & 0 \end{bmatrix} \begin{bmatrix} v \\ p \\ \phi \\ r \\ \psi \end{bmatrix} + \begin{bmatrix} 0 & 0.043 \\ 0.069 & 0 \\ 0 & 0 \\ 0 & 0.032 \\ 0 & 0 \end{bmatrix} \begin{bmatrix} \eta_c \\ \eta_{ped} \end{bmatrix}$$

Table 11 shows the stability roots, and it is clear that within the defined limits of identifiability, there has been little scope for reducing the instability of λ_{spiral}, the time to double amplitude increasing from 7.5 to 11.4 sec. The approximation for λ_{spiral}, if it retains its validity for all L_v, does indicate that the spiral mode will only stabilise for $L_v < 0$. —

Table 11 identified lateral/directional model stability roots, adjusted model

mode	eigenvalue
roll	-2.557
dutch roll	-0.515±1.393i
spiral	0.061

The impact of these adjustments on the verification result is shown in Figures 7 and 8. Improvement in medium- to long-term prediction of the response to rudder and lateral stick inputs is obtained relative to Figures 5 and 6. However, the impact of the unstable spiral mode is still evident in the response to a rudder input. There could be three reasons for this: firstly, the real aircraft may indeed have an unstable spiral mode, but it is not excited by the control inputs applied; secondly, the identified (linear) model is an incomplete description of behaviour, and slight non-linearity or coupling with other degrees of freedom is stabilising the spiral mode; thirdly, L_v could be poorly identified. The latter is highly unlikely, as the standard error

associated with the estimates is very small, indicating high confidence in the result. Similar values have been obtained from other events, Table 12.

Table 12 multi-run consistency in estimates of L_v

flight/event	estimate
flight 10/event 4	0.050 (0.004)
flight 10/event 11	0.058 (0.005)
flight 10/event 14	0.065 (0.005)

Data from steady heading sideslip tests is given in Figure 9, which shows lateral stick variation with sideslip angle at 70 mph, together with a best-fit through the measured data. The slope of the latter is -0.23 %/deg, or -0.30 %/deg if the measurement at 15 deg sideslip is discarded. From the rolling moment equation the rate of change of lateral stick with sideslip is given by

$$-\frac{L_v}{L_{\eta_c}} V_f$$

Substituting the identified values of L_v and L_{η_c} gives a value for the stick position versus sideslip gradient of -0.39 %/deg. These data confirm that L_v has been correctly identified with a positive sign, and hence, that the spiral mode is unstable for the other reasons outlined above.

Discussion

The results indicate that the VPM M16 gyroplane exhibits conventional lateral and directional dynamic stability characteristics. Features peculiar to this aircraft have rendered the robust identification of the stability and control derivatives a challenge. However informed application of system identification tools to the dynamic response data has been complemented by traditional flight test methods for steady data, resulting in a high degree of confidence in the results. Although specific to the VPM M16, the results can be interpreted in a more general context, as most contemporary light gyroplanes conform to the same configuration of open, streamlined pod for the occupants; a pusher propeller in close proximity to the fin and rudder, energising the airflow; and endplates on the tailplane.

The main rotor contributes the roll damping L_p and like a conventional helicopter, will have a very weak stabilising contribution to dihedral effect L_v . The absence of a tail rotor means that the basic airframe configuration dominates all the other stability derivatives. This includes the negligible value of L_r and N_p , which probably explains the very weak roll/yaw and yaw/roll coupling. Given the relatively low flight speed, the strong primary damping in yaw N_r is probably due to the energising effect of the propeller in close proximity to the fin and endplates. This parameter has been shown previously, Ref. 24, to have a dominant influence on dutch roll damping, and is primarily responsible for this mode being so well damped. The weathercock stability derivative N_v is of interest because it is stabilising and significant in magnitude. The concern with light gyroplanes of this configuration is the amount of side area ahead of the centre of mass, which will tend to be de-stabilising. Again, the energising effect of the propeller on the tail surfaces probably helps in this regard.

However, it is the result in dihedral effect L_v which is of the most interest. $L_v > 0$ tends to be de-stabilising, and its influence on the spiral mode is clear. Padfield, Ref. 24 has also shown that it can also adversely affect dutch roll stability. It influences the static behaviour of the aircraft, as evidenced by the steady heading sideslip results. Relative to light fixed-wing aircraft, where sideslipping flight such as crosswind operation means that right rudder requires left stick, $L_v > 0$ means that the lateral stick is required to move in the opposite sense. $L_v > 0$ results from the fact that the vertical areas on the aircraft are low on the airframe, relative to the centre of mass which is fairly high. All light gyroplanes seem to be of this configuration. The stabilising tendency of the rotor is very weak and the results here indicate that it is swamped by these airframe effects. The spiral mode behaviour is not fully understood, and the mechanism for it being stable in the light of the identified stability derivatives is not clear, and may not be repeated on other machines. However, by virtue of the similarity in configuration, $L_v > 0$ most probably is. A suitable and simple design improvement would be to add vertical area above the centre of mass, and the most expedient means of doing so would be to streamline the rotor mast.

Finally, the dynamic stability characteristics are such that this aircraft would easily satisfy the requirements of BCAR Section T. Indeed, against the requirements of the latest military rotorcraft handling criteria, Ref. 25, it would satisfy the requirements for Level 2 (acceptable) handling qualities in roll for most tasks, and easily meet Level 1 (satisfactory) criteria for dutch roll characteristics. It is unlikely therefore that the poor accident record of light gyroplanes is a consequence of lateral/directional stability and control characteristics.

Conclusions

Robust identification of gyroplane lateral and directional stability and control derivatives has been possible using relatively straightforward frequency-domain parameter estimation tools.

The results indicate that the basic design configuration of the contemporary light gyroplane does not compromise lateral/directional characteristics, although greater dihedral effect is possibly desirable.

The results are unique, and therefore contribute directly to the development of the UK gyroplane airworthiness and design standard, BCAR Section T in the important area of dynamic stability.

Acknowledgement

This work was conducted for the U.K. Civil Aviation Authority under Research Contract No. 7D/S/1125. The Technical Authority was Mr. David Howson.

References

1) Anon, "Airworthiness Review of Air Command Gyroplanes", Air Accidents Investigation Branch Report, Sept. 1991.

2). Anon, "British Civil Airworthiness Requirements, Section T, Light Gyroplane Design Requirements", Civil Aviation Authority Paper No. T 860 Issue 2, Jul. 1993.

3). Houston, S. S., "Longitudinal Stability of Gyroplanes", *The Aeronautical Journal*, Vol. 100, No.991, 1996, pp. 1-6.

4). Houston, S. S., "Identification of Autogyro Longitudinal Stability and Control Characteristics from Flight Test", University of Glasgow Dept. of Aerospace Engineering Report No. 9701, 1997.

5). Glauert, H., "A General Theory of the Autogyro", Aeronautical Research Committee Reports and Memoranda No. 1111, Nov. 1926.

6). Lock, C. N. H., "Further Development of Autogyro Theory Parts I and II", Aeronautical Research Committee Reports and Memoranda No. 1127, Mar. 1927.

7). Glauert, H., "Lift and Torque of an Autogyro on the Ground", Aeronautical Research Committee Reports and Memoranda No. 1131, Jul. 1927.

8). Lock, C. N. H., Townend, H. C. H., "Wind Tunnel Experiments on a Model Autogyro at small Angles of Incidence", Aeronautical Research Committee Reports and Memoranda No. 1154, Mar. 1927.

9). Glauert, H., Lock, C. N. H., "A Summary of the Experimental and Theoretical Investigations of the Characteristics of an Autogyro", Aeronautical Research Committee Reports and Memoranda No. 1162, Apr. 1928.

10). Wheatley, J. B., "Wing Pressure Distribution and Rotor-Blade Motion of an Autogyro as Determined in Flight", NACA TR 475, 1933.

11). Wheatley, J. B., "An Aerodynamic Analysis of the Autogyro Rotor with a Comparison Between Calculated and Experimental Results", NACA TR 487, 1934.

12). Wheatley, J. B., Hood, M. J., "Full-Scale Wind-Tunnel Tests of a PCA-2 Autogyro Rotor", NACA TR 515, 1935.

13). Wheatley, J. B., "An Analytical and Experimental Study of the Effect of Periodic Blade Twist on the Thrust, Torque and Flapping Motion of an Autogyro Rotor", NACA TR 591, 1937.

14). Schad, J. L., "Small Autogyro Performance", *Journal of the American Helicopter Society*, Vol.10, 1965.

15). McKillip, R. M., Chih, M. H., "Instrumented Blade Experiments Using a Light Autogyro", *Proceedings of the 16th. European Rotorcraft Forum,* Glasgow, Scotland, Sept. 1990.

16). Fu, K.-H., Marchand, M., "Helicopter System Identification in the Frequency Domain", *Proceedings of the 9th. European Rotorcraft Forum,* Sept. 1983.

17). Tischler, M. B., et al, "Demonstration of Frequency-Sweep Testing Technique using a Bell 214-ST Helicopter", NASA TM-89422, April 1987.

18). Tischler, M. B., "Frequency-Response Identification of XV-15 Tilt-Rotor Aircraft Dynamics", NASA TM-89428, May 1987.

19). de Leeuw, J. H., "Identification Techniques, Model Structure and Time Domain Methods", AGARD LS178, pp. 5-1 to 5-9, October 1991.

20). Kaletka, J., "Instrumentation and Data Processing", AGARD LS178, pp. 3-1 to 3-18, October 1991.

21). Tischler, M. B., "Identification Techniques, Frequency Domain Methods", AGARD LS178, pp. 6-1 to 6-4, October 1991.

22). Houston, S. S., Black, C. G., "On the Identifiability of Helicopter Models Incorporating Higher Order Dynamics", *AIAA Journal of Guidance, Control and Dynamics*, Vol. 14, No. 4, July-August 1991, pp. 840-847.

23). Murray-Smith, D. J., "Modelling Aspects and Robustness Issues in Rotorcraft System Identification", AGARD LS178, pp. 6-1 to 6-4, October 1991.

24). Padfield, G. D., "SA330 Puma Identification Results", AGARD LS178, pp. 10-1 to 10-38, October 1991.

25). Anon, "Handling Qualities Requirements for Military Rotorcraft", US Army ADS-33D, July 1994

Figure 1 -- VPM M16 gyroplane instrumented for flight trials

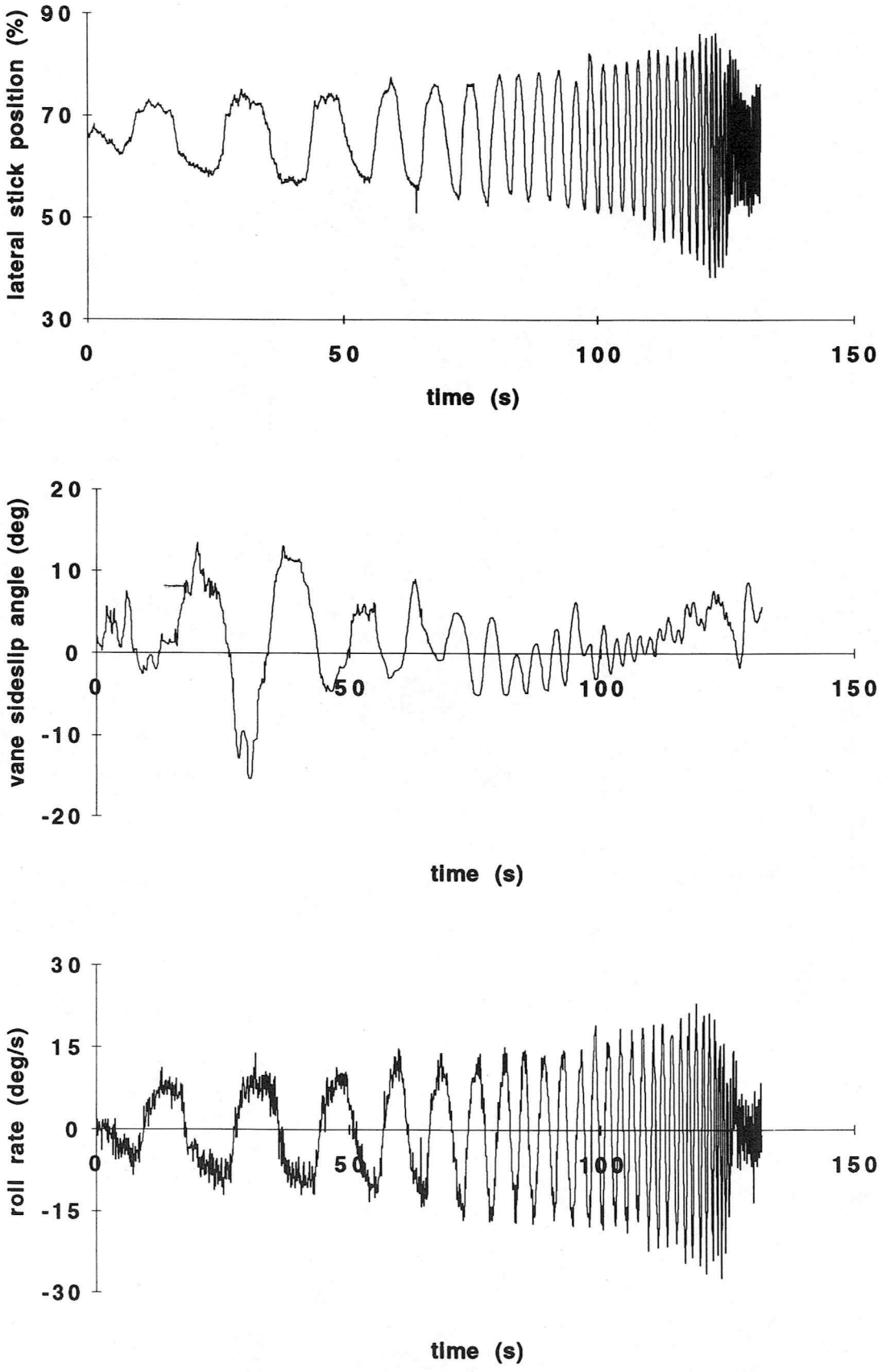

Figure 2 -- Lateral stick frequency sweep

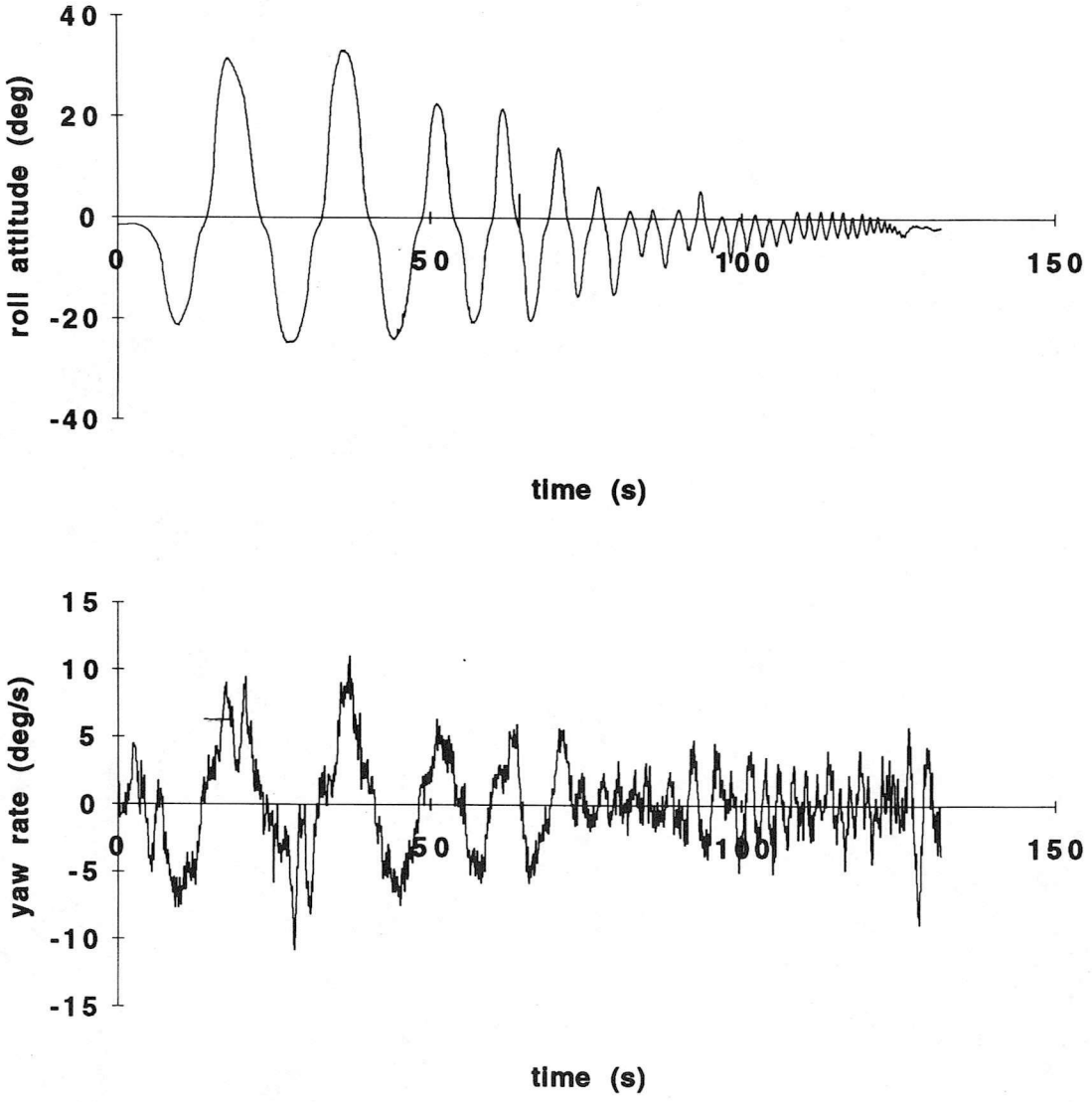

Figure 2 (concl.) -- Lateral stick frequency sweep

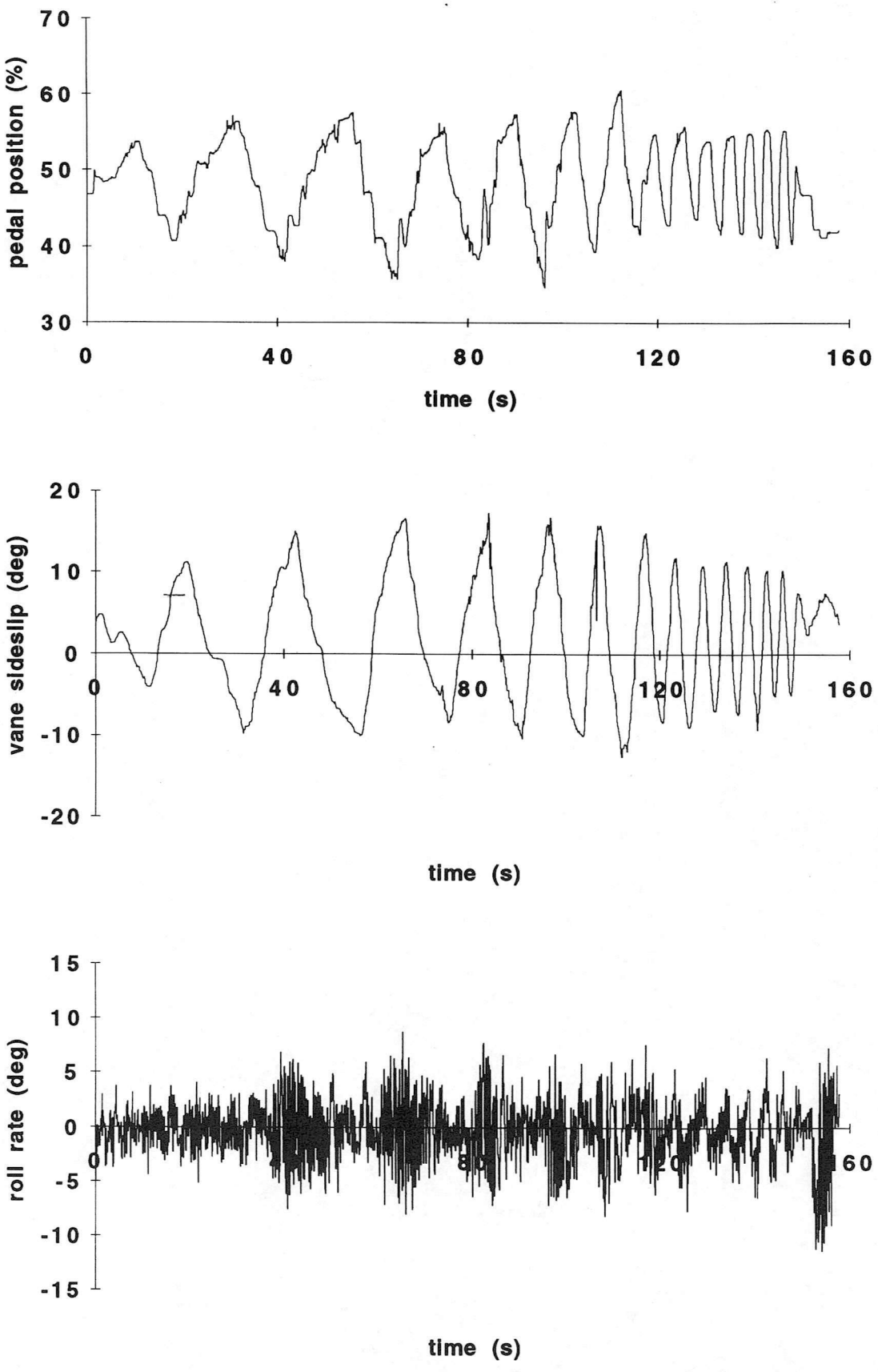

Figure 3 -- Rudder pedal frequency sweep

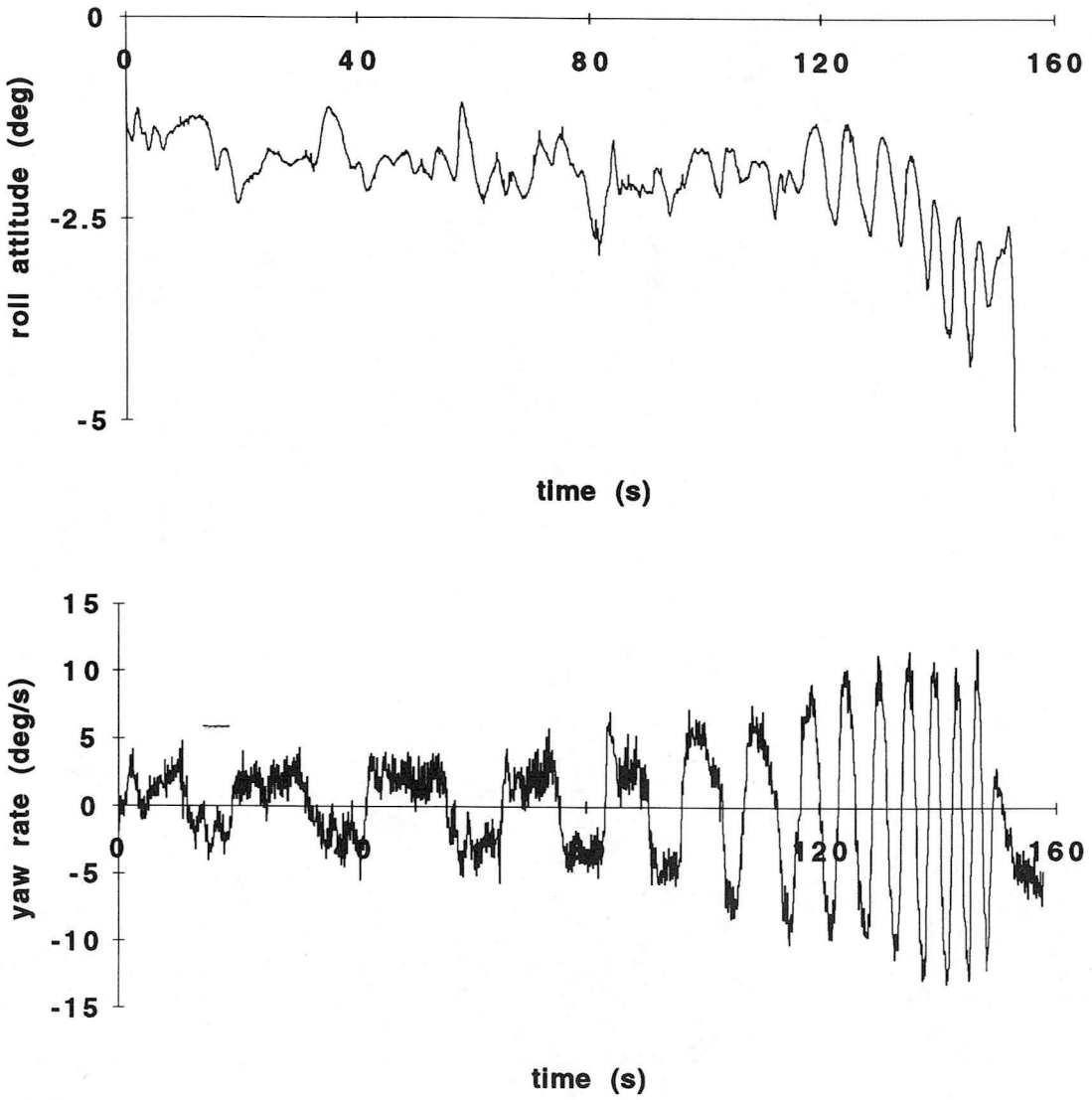

Figure 3 (concl.) -- Rudder pedal frequency sweep

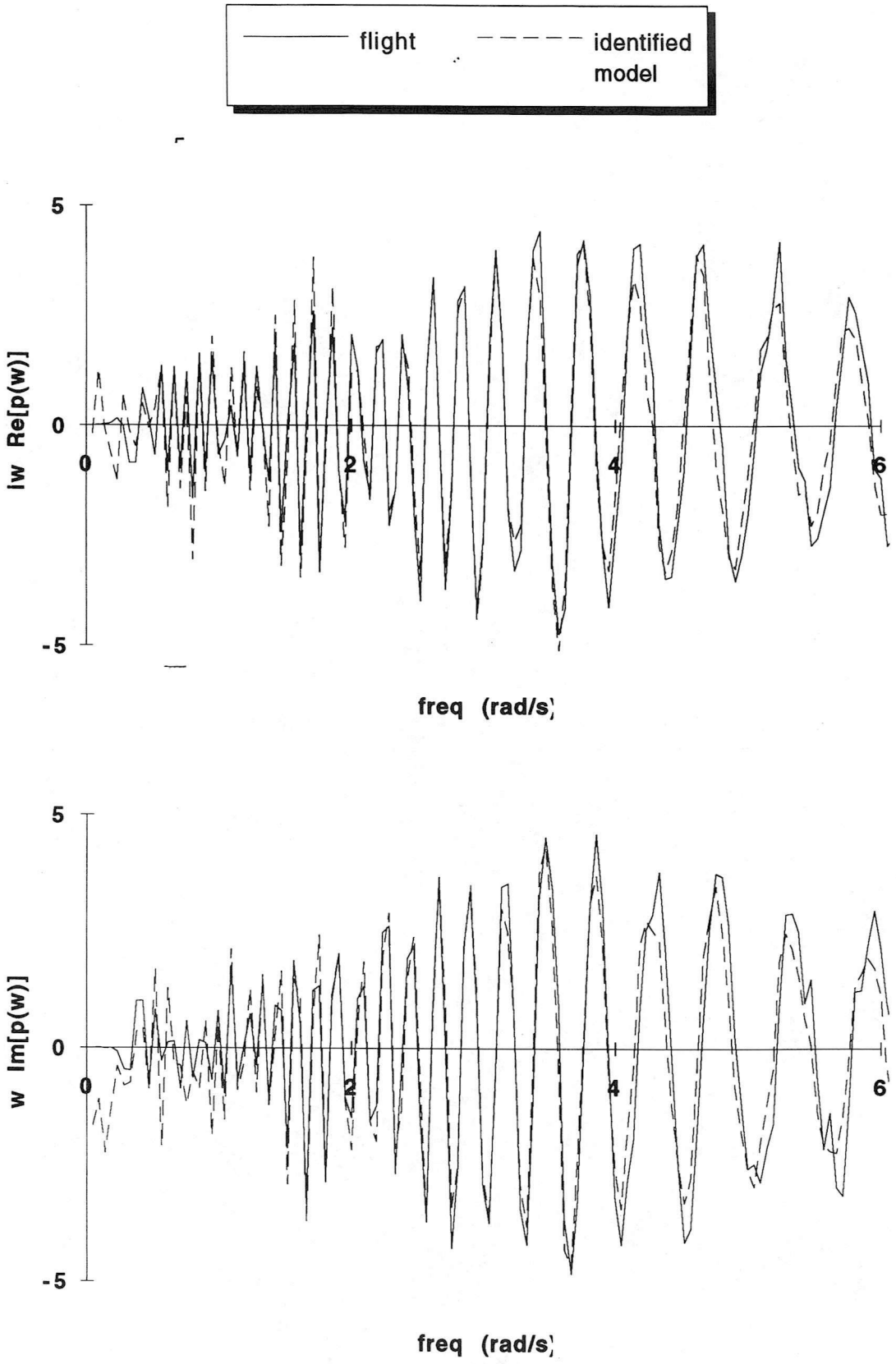

Figure 4 -- Comparison of flight and identified model roll moment

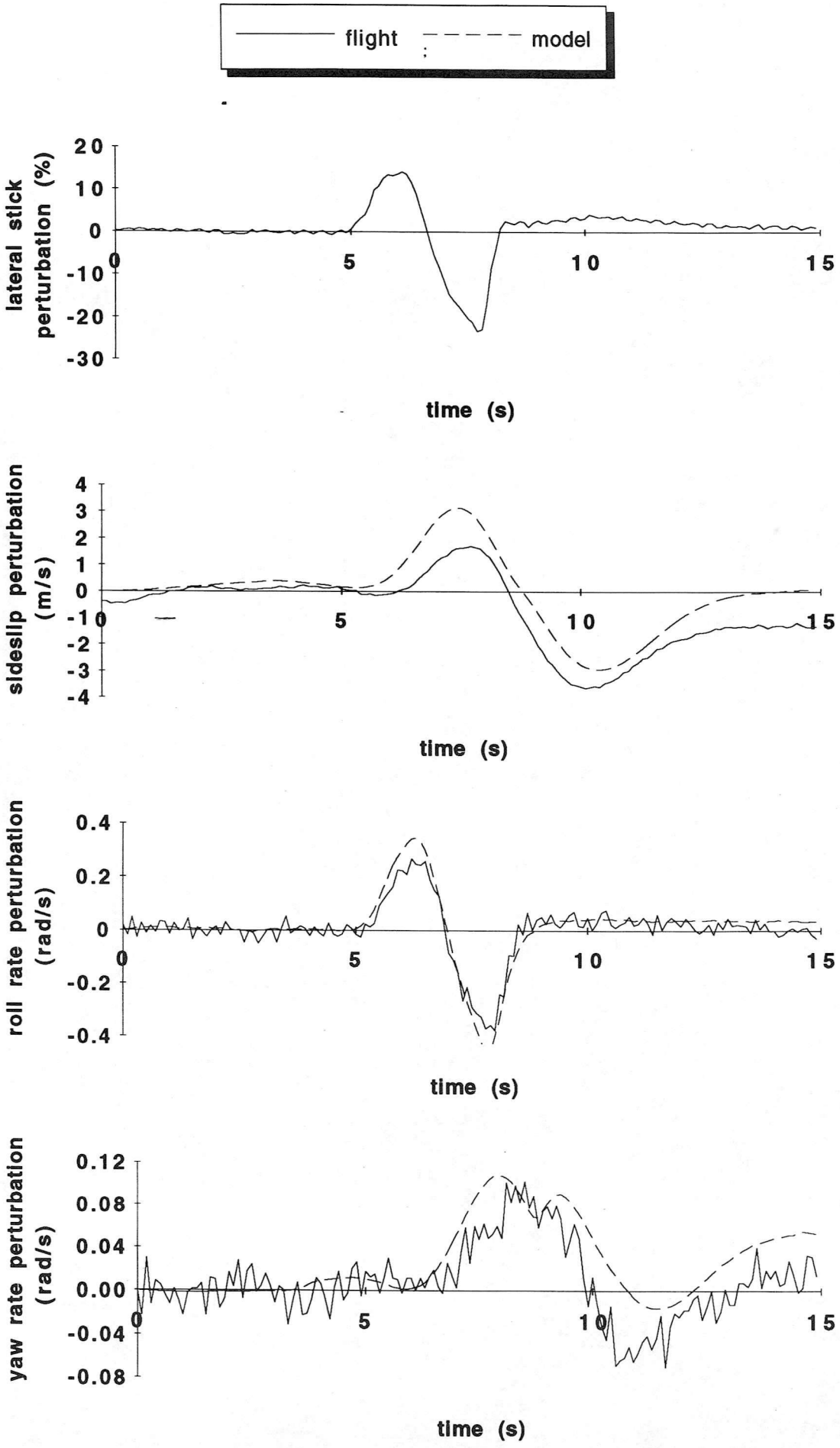

Figure 5 -- Identified model verification - lateral stick input

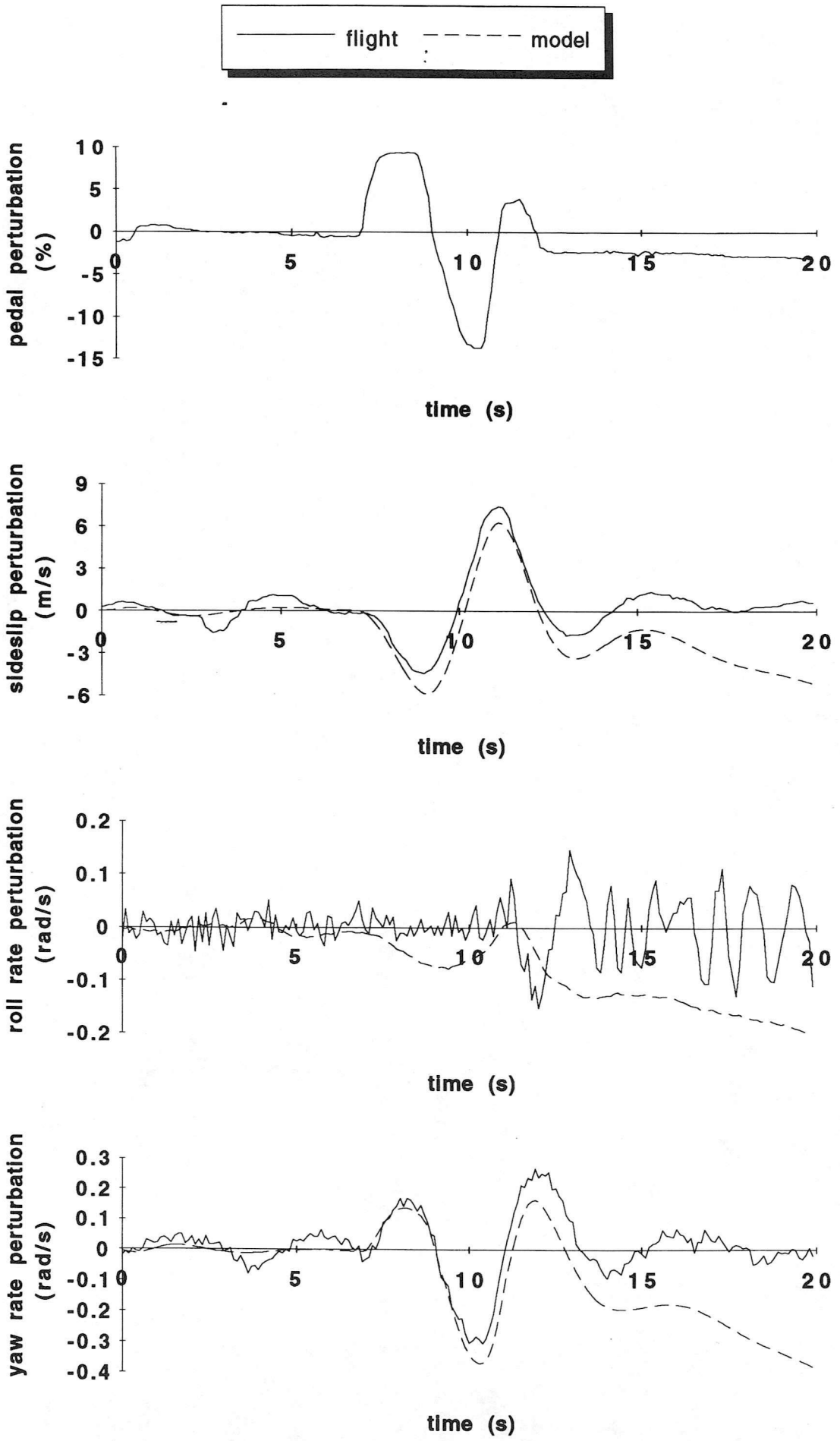

Figure 6 -- Identified model verification - rudder pedal input

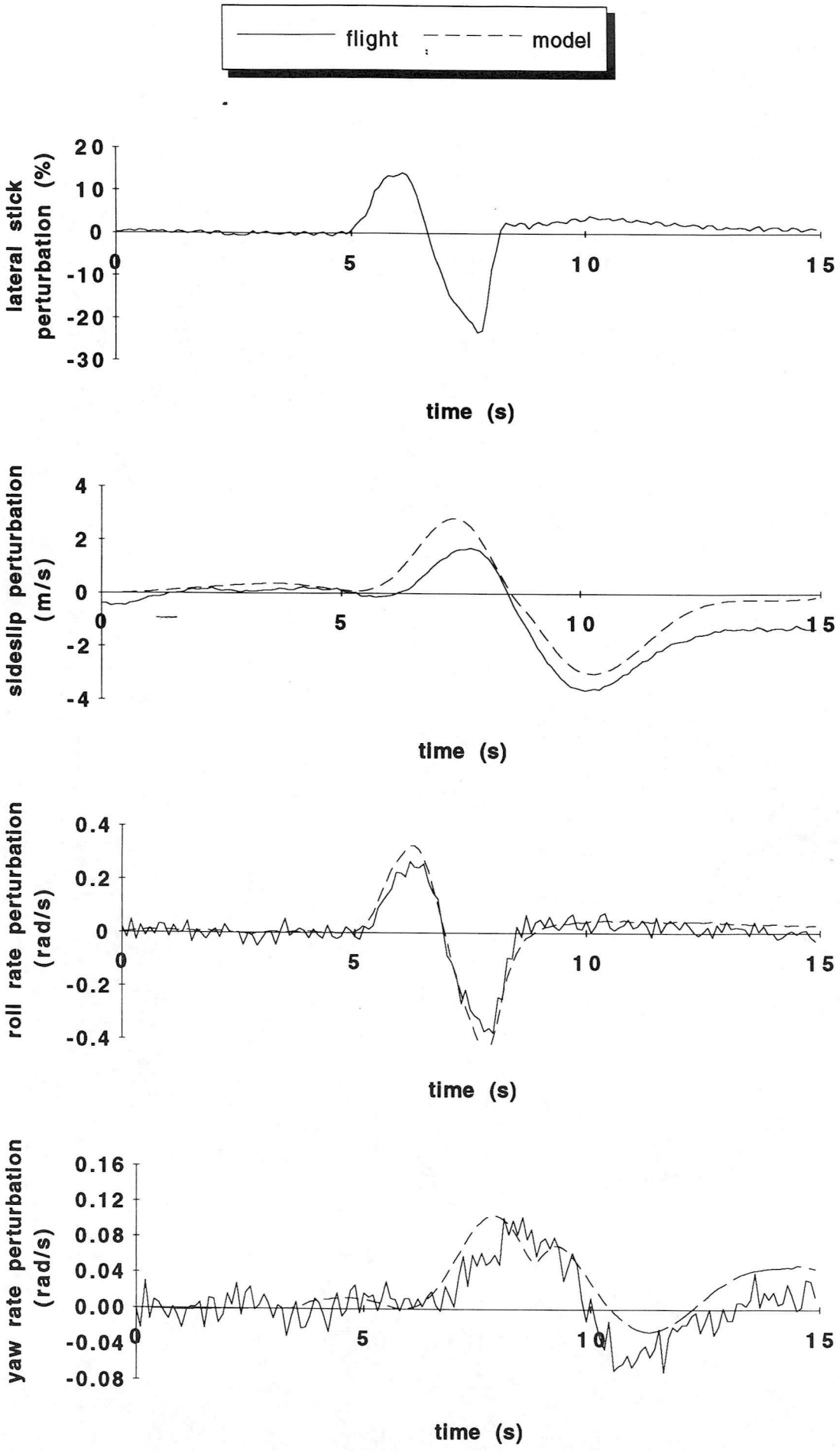

Figure 7 -- Adjusted model verification - lateral stick input

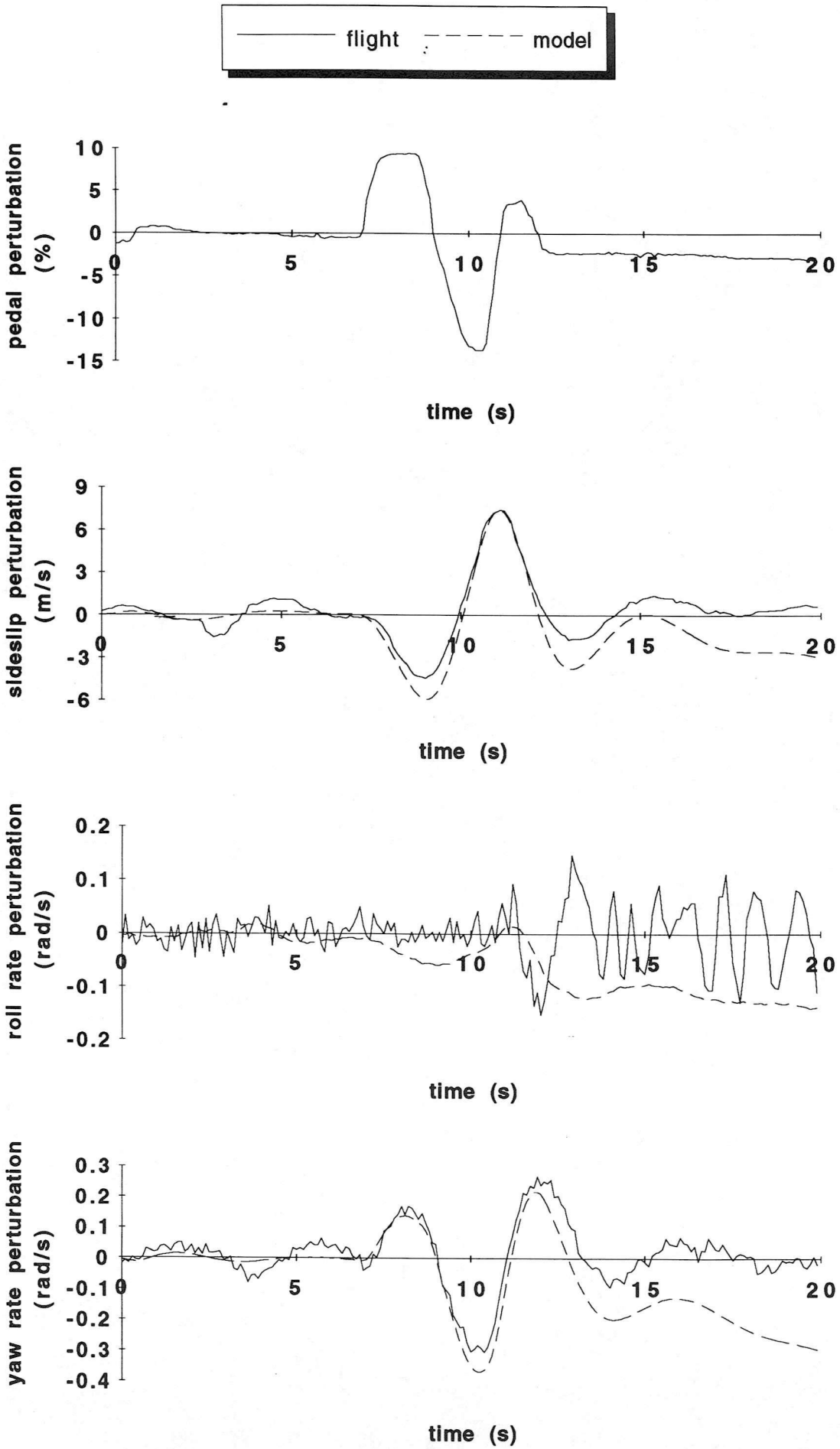

Figure 8 -- Adjusted model verification - rudder pedal input

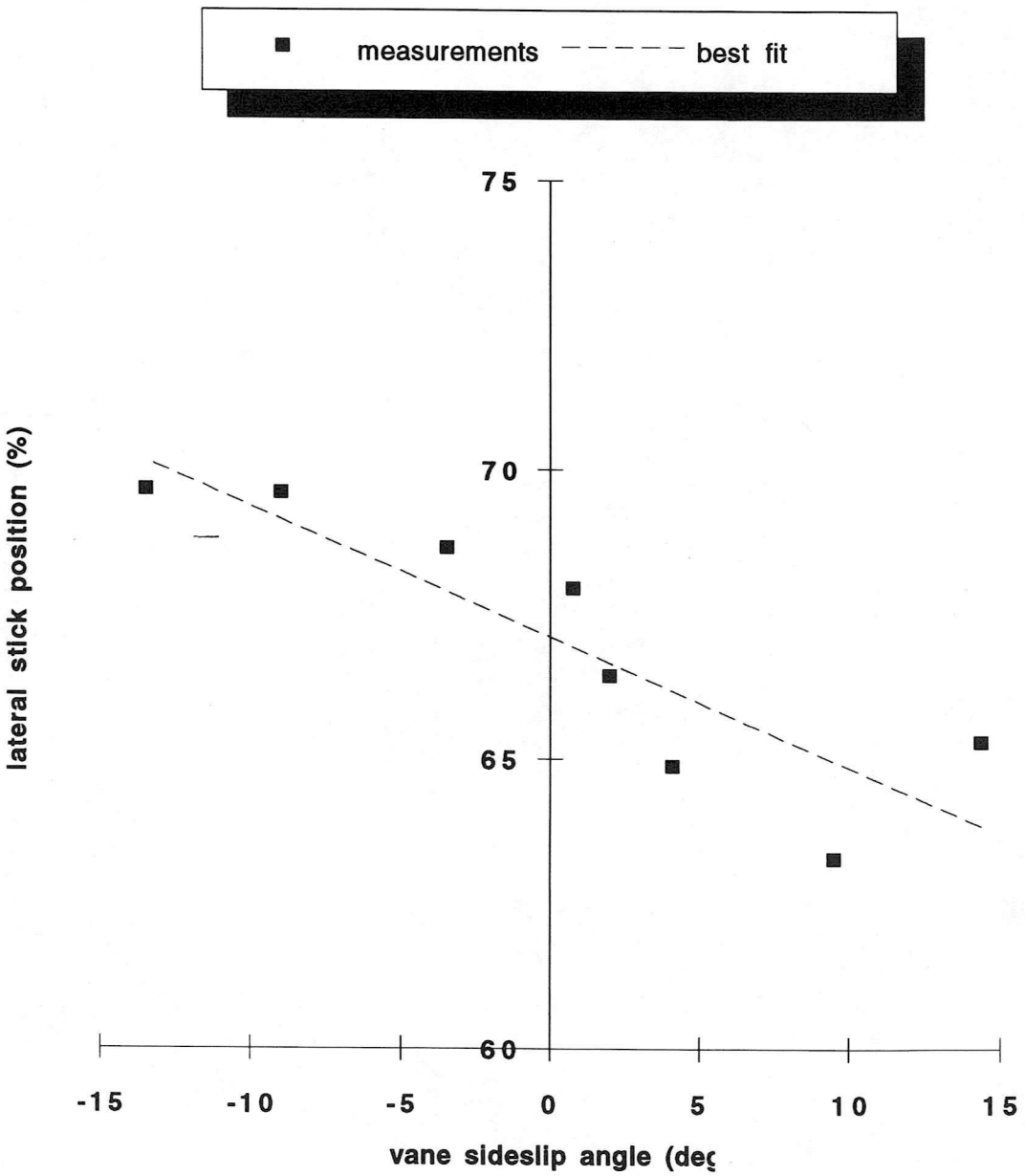

Figure 9 -- Lateral stick position with sideslip